Supporting Information

1. Experimental Methods

All of the experiments presented here were performed on [0001] oriented 99.999% pure Mg single crystal, loaded in the [0001] direction. For conventional bulk counterpart, $\{10\bar{1}2\}<10\bar{1}\bar{1}>$ extension twinning is favored under tension, and $\{10\bar{1}1\}<10\bar{1}\bar{2}>$ contraction twinning is expected under compression. Basal slip and prismatic slip systems are suppressed since their corresponding critical resolved shear stress (CRSS) are zero. Pyramidal slip is also difficult to activate at room temperature due to its low CRSS.

Submicron-sized tension, compression and bending specimens were fabricated with a FEI Strata 235 Dual Beam Focus Ion Beam (FIB). A Fischione 1040 NanoMill with Ar^+ source was used afterwards to remove the damage layer induced by FIB. Figure S1 below shows the typical TEM images of tension, compression and bending samples before testing, respectively. The diffraction patterns inset confirm the orthogonal orientation of samples so that loading is always in the [0001] direction. The tensile samples were fabricated to be 2-3 μm long, 100-200 nm wide and about 150 nm in thickness; bending samples were 1-2 μm long, about 200 nm in width and about 150 nm in thickness; compression samples were made approximately 200 nm in diameter. The *in situ* TEM uniaxial tensile tests, bending tests and compression tests were performed along the [0001] direction in a JEOL 3010 TEM with a Hysitron Picoindenter. The diamond tensile tip was fabricated by FIB to have a gripper gage size ~500 nm. For compression and bending a flat punch was used that had a diameter ~5 μm, also fabricated by FIB. All of the tests were conducted under displacement control mode with displacement rate of 10 nm/s. After the *in situ* tensile and bending tests the sample was further thinned down for high-resolution TEM (HRTEM) imaging with a 2kV Ar^+ ion beam. HRTEM study of the atomic structure of the twin was performed with a Philips CM300FEG TEM at 300KV and a FEI Technai F20 at 200kV.

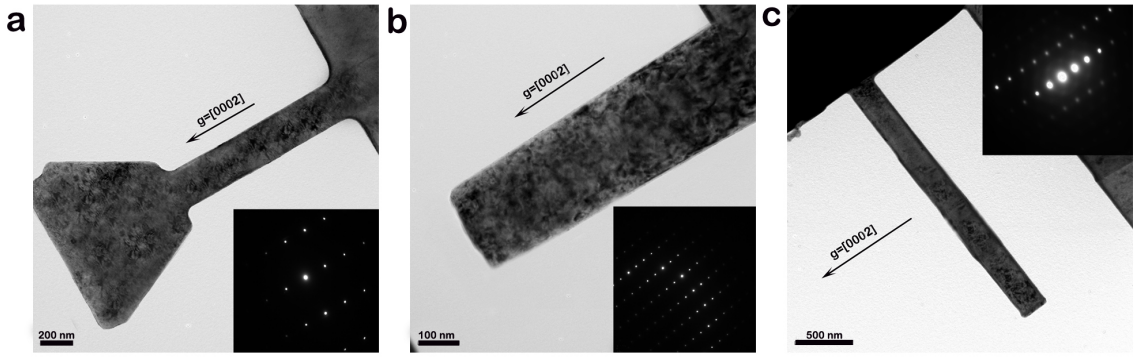

Figure S1. *The TEM bright field images of the samples before test. (a) tensile sample, (b) compression sample, (c) bending sample. The diffraction conditions are all g=[0002].*

In situ **Tensile, Bending and Compression Tests**

Figure S2 shows bright field TEM images at low magnification demonstrating alignment of the tensile gripper and sample. To perform the alignment, the sample and the tensile gripper were first brought to eucentric height using the aid of the microscope focus (shown in Figure S2a) when these two were out of contact. The gripper was then lowered along the Z-axis and moved forward along the X-axis to be right under the sample, and then raised back to eucentric height and adjusted along the X and Y axes simultaneously until the gripper was aligned with the sample but still out of contact, as shown in Figure S2b. Tensile testing could then be performed under displacement control in the negative X direction.

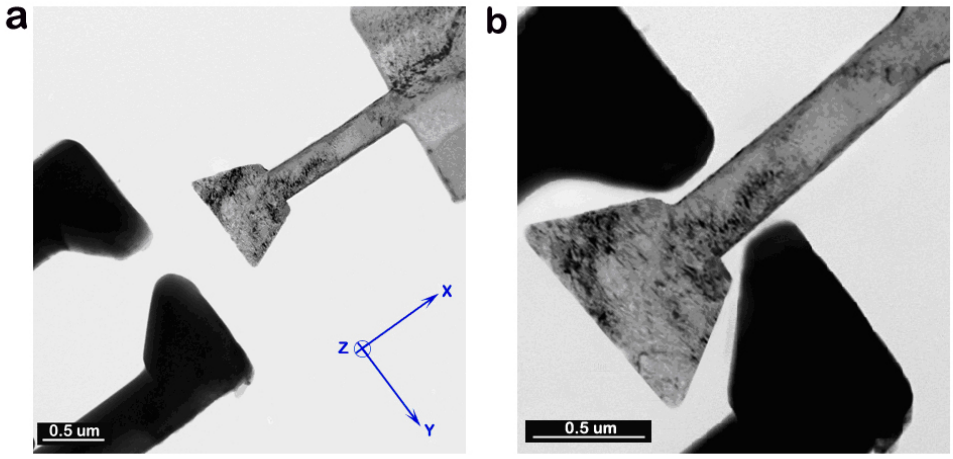

Figure S2 *The TEM image shows the position of the tensile sample and the gripper. (a) before alignment. (b) after alignment.*

The bending and compression tests were both performed with a flat punch in displacement control. Details regarding the *in situ* compression test can be found in another reference[3]. The bending tests were performed in a similar manner but contact was made at the end of the sample in a bending configuration.

2 Compression Results

The deformation twinning behavior observed under compression does not generate a nanotwinned structure as the cases of tension or bending. Figure S3a shows a dark field image of the twinned sample post-compression. X-ray microdiffraction analysis (Figure S3b and c) revealed the appearance of a $\{10\bar{1}1\}$ contraction twin and large number of dislocations. From the *in situ* video, it was found that a twin formed from the top corner of the sample first and then the twin boundary gradually moved forward under loading, accommodating dislocation activities within the twin and near the boundary. The result was the growth of a continuous twin, producing a shear displacement (marked in red in Figure S3a). HRTEM study showed the bulk twin structure and no nanotwinned structure was found (see HRTEM image inset in Figure S3a). Unlike the generation of the nanotwinned structure, the compression test provides a good example of preferred

nucleation and growth of the twin due to stress concentrations at the contact surface and the tapered geometry.

The twin type was also confirmed and the induced dislocation structures were investigated by using synchrotron based x-ray Laue microdiffraction (mXRD) technique on Beamline 12.3.2 at the Advanced Light Source of the Lawrence Berkeley National Laboratory. A high brilliance synchrotron polychromatic x-ray beam (5-24 keV) is focused down to 1 mm^2 size by a pair of Kirkpatrick-Baez mirrors. The Mg nanopillar after compression was positioned at the x-ray focal point and a Laue diffraction pattern was recorded by a MAR133 x-ray CCD (MARCCD) detector in reflection geometry. The sample and the CCD detector were tilted by 45^o and 90^o with respect to the micro-focused x-ray beam, respectively. The distance from the sample to the center of the MARCCD was about 78 mm. The experimental geometry was calibrated by recording a Laue diffraction pattern on a strain-free Si chip. The Diffraction pattern was indexed using the software package XMAS[2]. By comparing the orientation matrices, it was found that the tilt angle between the matrix and twin domains was 56.4^o along $[11\bar{2}0]$ direction, which was close to the calculated angle (56.2^o) based on the unstrained lattice parameters corresponding to $(\bar{1}011)$ compression twin. Diffraction peaks from the matrix were observed to be split (Fig S3b), which indicated that geometrically necessary dislocations (GNDs) were aligned and two subgrains were formed after the compression load. Detailed study of the subpeaks revealed that the tilt angle between the two subgrains was about 1.1^o, and the GNDs were $[10\bar{1}0]$ direction.

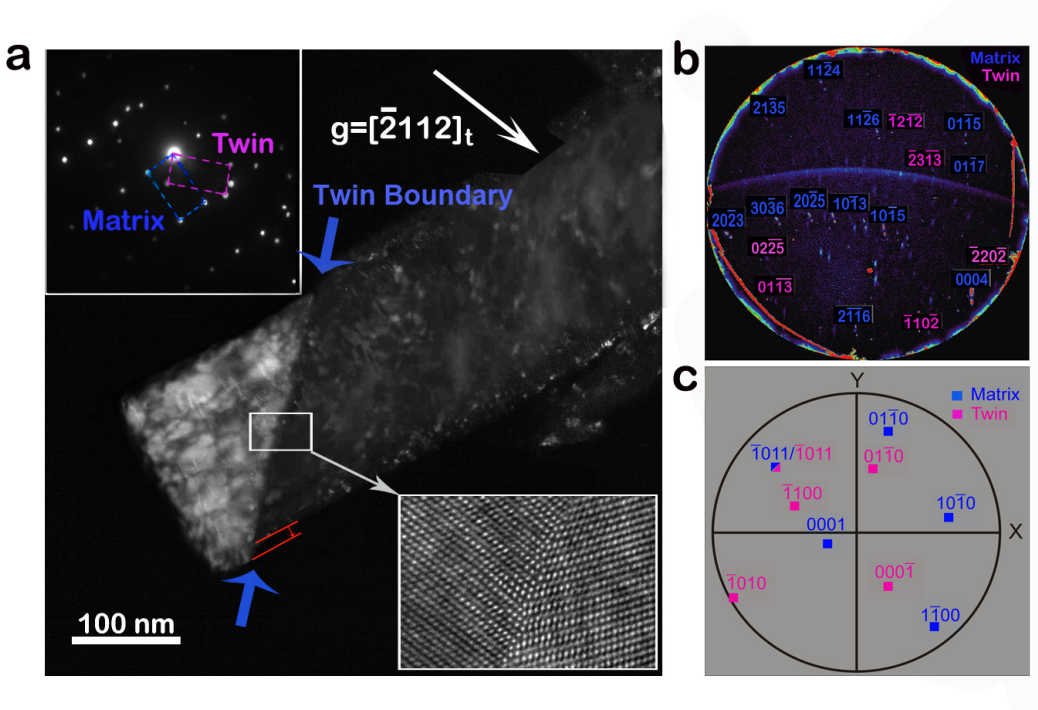

Figure S3| *TEM images and Laue diffraction data from an in situ compression test of [0001] oriented Mg. (a) A dark field image showing the in situ compression sample post-deformation, the diffraction condition is g=* $[\bar{2}112]_t$ *. The twin boundary is indicated by blue arrows, and the shear displacement is marked in red. One typical HRTEM image of compression sample is inserted showing the* $\{10\bar{1}1\}$ *twinning structure. (b) mXRD pole figure of the compressed sample. Indexes labeled in blue are from the matrix and those in red belong to the twin. (c) A pole figure showing the corresponding planes of the matrix and the twin.*

3 HRTEM Image of extension Twin at the Crack Tip

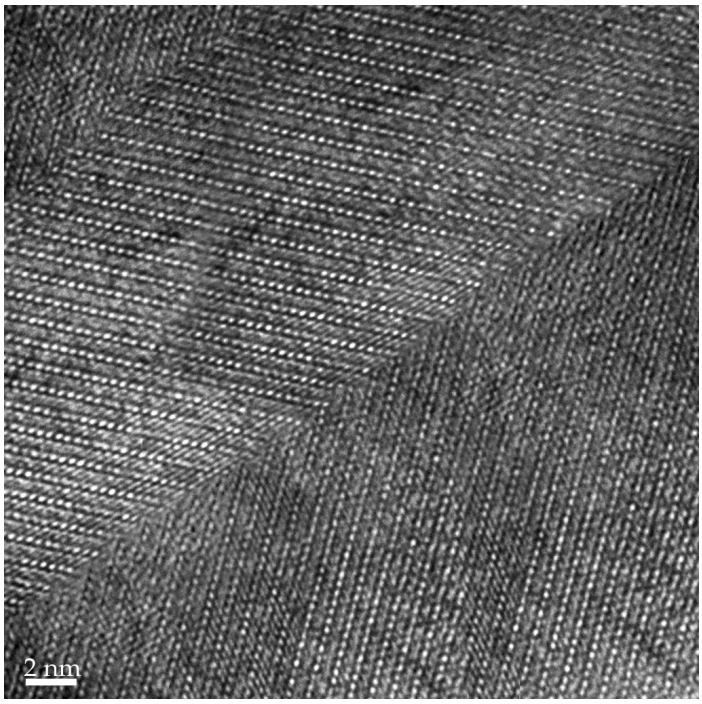

Figure S4 *The HRTEM image showing the nanotwinned structure with the extension type at the crack tip, which is corresponding to Figure 3 b in the main paper. ZA= [1-210].*

4 Deformation twinning and twin embryos in larger Mg samples

We also studied the deformation twinning in single crystal Mg bulk samples and micron-sized samples. Multiple deformation twins were found in both cases. The thickness of twins in bulk samples can be as large as hundreds nanometers and in micron-sized samples, the largest one we found is about 100 nm thick. In micron-sized samples, nanotwins were also found near the sample surface. One example is shown in Figure S5a. In this image, we can see there are several thick twins but also many small twins with thickness around several nanometers. We also observed the nano-sized twin embryos from the inside of the bulk sample as shown in Figure S5b. They were in the lens shape with thickness also around several nanometers.

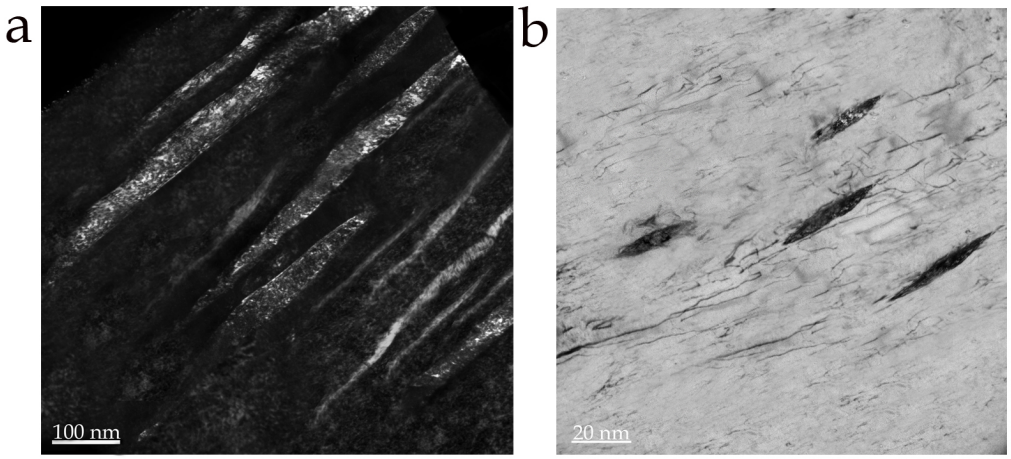

Figure S5 (a) The dark field image that shows the deformation twins in micron-sized sample, which was taken from the surface region of the sample. There are several big twins but also many nanotwins with thickness around several nanometers. (b) The bright field image that shows the twin embryos from inside of the bulk single crystal Mg sample, where the twin thickness is also around several nanometers.

4 Movies

There are three *in situ* TEM movies for each of the three tests described above and two simulation movies included in Supporting Information. Figure S6a, b and c below show the first frame of each of the three *in situ* TEM movies, respectively.

Movies:

1 Compression

http://mm.seas.upenn.edu/ql/www/Manuscript/Yu11/Movie/compression.mp4

2 Tension

http://mm.seas.upenn.edu/ql/www/Manuscript/Yu11/Movie/tension.mp4

3 Bending

http://mm.seas.upenn.edu/ql/www/Manuscript/Yu11/Movie/bending.mp4

4 kMC Simulation *(blue: matrix; red: twin)*

http://mm.seas.upenn.edu/ql/www/Manuscript/Yu11/Movie/kMC.avi

5 MD Simulation

http://mm.seas.upenn.edu/ql/www/Manuscript/Yu11/Movie/Nucleation.avi

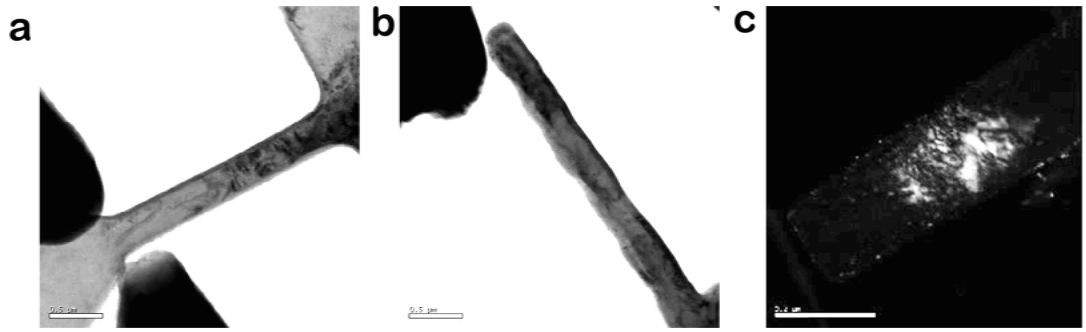

Figure S6 *The first frame of three in situ TEM movies (a) tension, (b) bending, (c) compression.*

6. Molecular Static Simulation for Stress Field of Nanotwin

A molecular static simulation was performed by LAMMPS with EAM interatomic potential for Mg[4]. 400000 atoms were used in a 210 nm × 172 nm × 0.32 nm box with free surfaces on both x ($<10\bar{1}\bar{1}>$) and y (perpendicular to $\{10\bar{1}2\}$ plane) directions but periodicity along z direction. A nanotwin (20 nm along $<10\bar{1}\bar{1}>$ direction and 4 nm perpendicular to $\{10\bar{1}2\}$ plane) was produced from the surface by continuous slip of $\{10\bar{1}2\}$ planes with Burgers vector of 0.49 Å along $<10\bar{1}\bar{1}>$ direction[5]. Both top and bottom $\{10\bar{1}2\}$ planes were fixed so that total engineering shear strain along $<10\bar{1}\bar{1}>$ direction was 0.01. Under such constrain, conjugate gradient relaxation was performed in order to reach the local minimum state. The distribution of atomic shear stress σ_{xy} was calculated and shown in Figure 4a of the main manuscript.

7. Kinetic Monte Carlo Simulation

A kinetic Monte Carlo simulation was performed based on a 2-D twinning dislocation (TD) model shown in Figure 4c of the main manuscript. There are three types of possible

events: TD nucleation on the atomic plane adjacent to existing twin boundary (TB), TD nucleation far from TB and TD migration on one atomic plane (no TD climb allowed). TD nucleation rate is written as a typical Arrhenius relation

$$\nu = \nu_0 \cdot \exp(-\frac{Q(\sigma)}{k_B T}) \quad (1)$$

Here we set $\nu_0 = 1\times10^{13}$ s^{-1} and T = 300 K. $Q(\sigma)$ is assumed to be linearly dependent on σ_S, the local shear stress field generated by both external shear strain and all TD, as

$$Q(\sigma) = Q_0 - \sigma_S \cdot \Omega \quad (2)$$

Here Ω is defined as activation volume. TD nucleation on existing twin boundary (TB) would have less Q_0 than those far from TB, because in the former case there is no new TB production. Here we set Q_0 = 0.60 eV for the former and 0.85 eV for the latter. Ω is set as 115 $Å^3$. At each nucleation and migration event, TD moves forward on the slip plane by one lattice spacing. Here the lattice structure and slip system of $\{10\bar{1}2\}<10\bar{1}\bar{1}>$ of Mg are applied so that each time TD migrate by 7.61 Å, and the distance between adjacent slip planes is d_{SP} = 3.80 Å. The migration rate is also assumed to be linearly dependent on the applied stress:

$$\nu_S = M \cdot \sigma_S \quad (3)$$

We then set M = 2000 $Pa^{-1}\bullet s^{-1}$ so that the average glide velocity of TD under shear stress σ_S = 500 MPa is approximately 1000 m/s. σ_S is generated by the fixed external shear strain, TD and their surface images. The shear stress field of single TD or TD surface image is described by classical dislocation elastic theory as

$$\sigma_{xy} = \frac{Gb_{TD}}{2\pi(1-\nu)} \cdot \frac{x(x^2-y^2)}{(x^2+y^2)^2} \quad (4)$$

where x is coordinate along slip direction and y is along direction perpendicular to slip plane. G is shear modulus; here we set G as 19 GPa from first-principles calculations under the slip system of $\{10\bar{1}2\}<10\bar{1}\bar{1}>$ of Mg[6]. b_{TD} is the Burgers vector of TD and equal to 0.49 Å for $\{10\bar{1}2\}<10\bar{1}\bar{1}>$ twin, and it changes the sign for TD surface images[5]. Poisson's ratio is 0.3 here.

The size of simulation cell is 200 nm along $<10\bar{1}\bar{1}>$ direction and 760 nm

perpendicular to $\{10\bar{1}2\}$ plane. The external engineering shear strain is fixed as $\gamma = 0.03$, and the external shear stress is calculated as

$$\sigma_S^{ext} = G\,\gamma \cdot (1 - \frac{V_{Twin}}{V_{Tot}} \cdot \frac{b_{TD}}{d_{SP}}) \quad (5)$$

where V_{Twin} and V_{Tot} is the volume of deformation twinning and total simulation cell. So the total shear stress at each investigated point is

$$\sigma_S = \sigma_S^{ext} + \sum \sigma_{xy} \quad (6)$$

where the summation is performed upon each TD and its two images on both surfaces. 130000 simulation steps were performed and the result is shown in movie 4. The final configuration and time evolution of σ_S^{ext} are shown in Figure S7 (a) and (b). The thickness and spacing of nanotwins are close to experimental observations. The time evolution of σ_S^{ext} suggests that there are three stages of the formation of nanotwinned structure: stage I: nucleation of multiple nanotwins in a very short time; stage II: growth of nanotwin thickness by TD nucleation and glide on existed TB; stage III: near-constant nanotwin thickness when σ_S^{ext} significantly decreases as Eq. (5).

To illustrate the effect of the TD elastic field on nanotwin nucleation, we performed another simulation, where the nucleation rate on the surface is independent of the TD elastic field but all the other parameters are the same. Compared with Figure S7 (a), the result in Figure S7 (c) shows that the number of nanotwins decreases and the average thickness of individual twins increases significantly. This suggests that the correlation between nucleation and TD elastic field is a critical factor for the formation of nanotwinned structure.

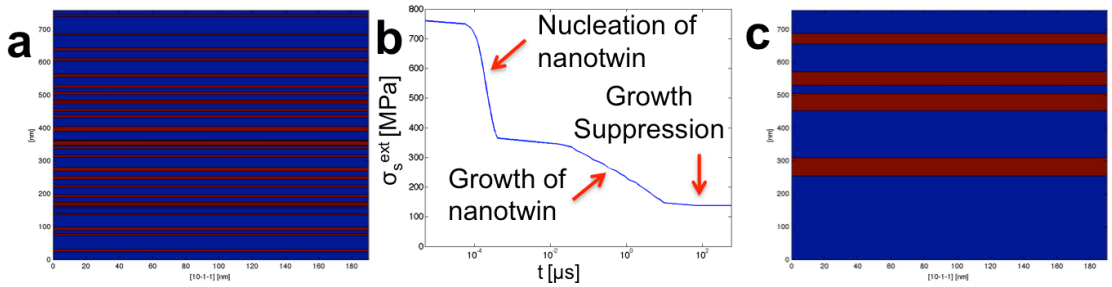

Figure S7 (a): *Final configuration (blue: matrix; red: twin) of simulation. (b): Time evolution of* σ_S^{ext}. *(c): Final configuration of simulation result when TD nucleation rate at surface isn't affected by TD stress field.*

8. Molecular Dynamic Simulation for Twin Nucleation in Tensile Tests

Molecular dynamics simulations were performed by LAMMPS to investigate the nucleation mechanism of deformation twinning in tensile tests of Mg single crystal along $<0001>$ direction, and two different EAM interatomic potentials for Mg[4,7] were applied to reach consistent results. MD samples were made into rectangular shapes with perpendicular x ($[2\bar{1}\bar{1}0]$), y ($[01\bar{1}0]$) and z ($[0001]$) axis, respectively, and periodic boundary condition along z-axis. All the tensile tests were performed at temperature of 300 K and MD relaxation of 1 nano-second under 300K was performed before each tensile test. We have tested samples with different sizes, strain rates (10^6 s^{-1} – 10^{10} s^{-1}), surface conditions (clean without vacancies and rough with high concentration of vacancies) and EAM potentials. All the results show that deformation twins nucleate from the edges between the intersections of two facets, and the critical stress for twin nucleation should be in the range of 600~1000 MPa under the strain rate of ~10^{-2} s^{-1} (the strain rate in real experiments) from extrapolation approximations (Details in the following paragraphs), which explains the origin of high stress of twin nucleation observed in the experiments.

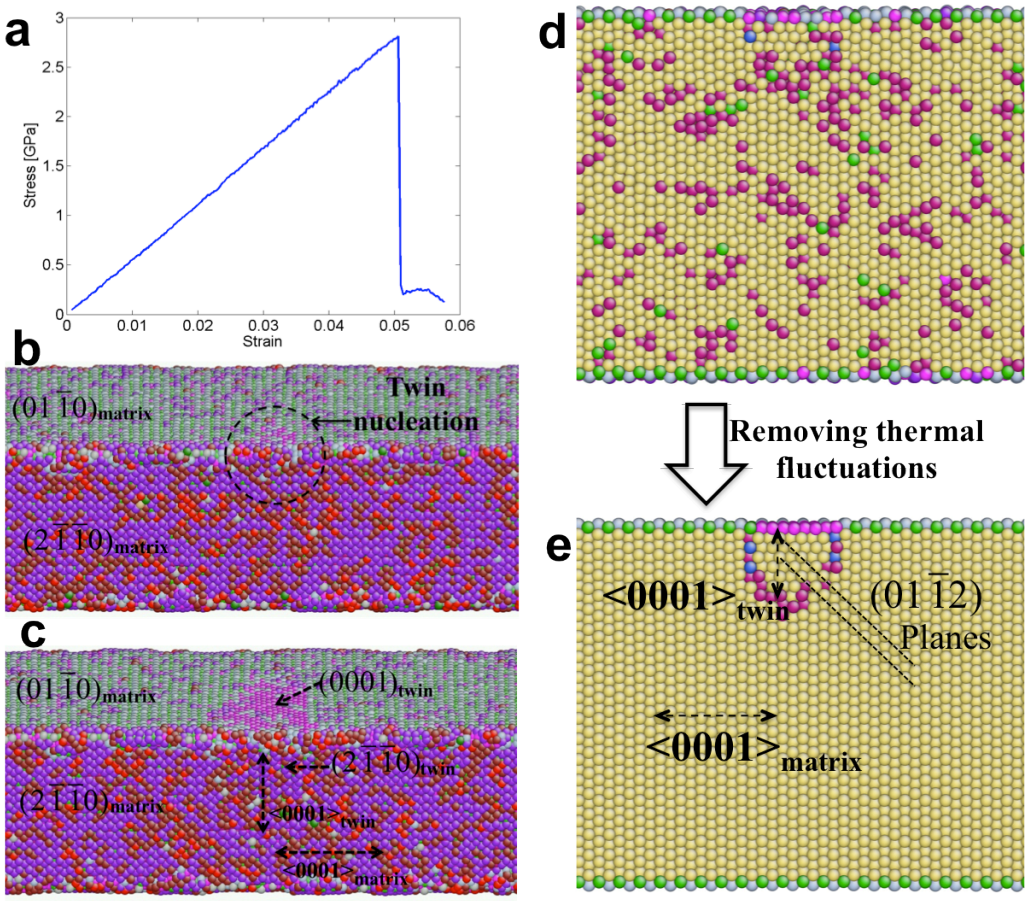

Figure S8 (a) Stress-strain curve for MD tensile test of 10 × 10 × 30 nm^3 sample with clean surfaces at T = 300 K and under strain rate of 2 × 10^7 s^{-1}. Mg EAM potential from Ref. 4 was applied. (b) and (c): Nucleation and propagation of extension twin embryo on the edge between two facets at the critical stress obtained from MD simulations. Here two different surfaces of the sample are shown and different colors mean different coordination number (CN) of atoms (yellow: CN = 12 for Mg in bulk lattice; magenta: CN = 9 for Mg on (0001) surface). The local variations of CN numbers result from thermal fluctuation at T = 300 K. (d): Cross section of a $(2\bar{1}\bar{1}0)$ *plane near the sample surface after twin nucleation. (e): 50 steps of conjugate gradient relaxation were performed to the MD configuration of (d) to remove the effect of thermal fluctuation in order to obtain a clear illustration. The boundaries between twin and matrix are partial dislocations on* $(01\bar{1}2)$ *planes, as shown on the tilted dashed lines. The <0001> directions of the matrix and the twin are almost perpendicular to each other, which is the*

typical character of $\{10\bar{1}2\}\langle 10\bar{1}\bar{1}\rangle$ type of extension twin.

Figure S8 shows the detailed results for MD tensile test of 10 × 10 × 30 nm^3 sample with clean surfaces under strain rate of 2 × 10^7 s^{-1}. In Figure S8 (a), the stress-strain curve initially behaves as a straight line with slope of 56 GPa. When the stress reaches 2.8 GPa, it suddenly drops to almost zero, corresponding to the nucleation and growth of deformation twin as shown in Figure S8 (b), (c) and movie 5, where the twin is nucleated from the edge between two surfaces ($(2\bar{1}\bar{1}0)$ and $(01\bar{1}0)$). To obtain a clear picture of the twin type and formation mechanism, a cross section near $(2\bar{1}\bar{1}0)$ surface is plotted in Figure S8 (d) and (e), which clearly show that this twin embryo is $\{10\bar{1}2\}\langle 10\bar{1}\bar{1}\rangle$ type of extension twin, composed by partial dislocations on $\{10\bar{1}2\}$ planes.

However, the critical stress for the twin nucleation (2.8 GPa) from the above calculation is too high compared with our experimental value (~800 MPa). We believe it mainly results from two factors: surface defects and strain-rate effects. In real experiments, all samples are produced by FIB processing and following high-energy Ar^+ cleaning, so the surface should be very rough with high concentration of defects. These defects could facilitate the nucleation process and decrease the critical stress. Meanwhile, the strain-rate in MD (~10^7 s^{-1}) is much higher than that of real experiments (~10^{-2} s^{-1}), which also significantly change the critical stress values. Thus we first produced MD samples with rough surfaces, as shown in Figure S9 (a), where the surface roughness was made by superpositions of sinusoidal waves plus random-noise perturbations. Then samples with different sizes and surface conditions (clean and rough) were calculated under different strain rates (from 10^6 s^{-1} to 10^{10} s^{-1}) and EAM potentials. We expect the critical stress and the strain rate have certain power-law relations, thus we plot the $\log_{10}$(critical stress) vs. $\log_{10}$(strain rate) in in Figure S9 (b) and extrapolate them into the regions of low strain rates. The results show that the surface defects can lower the critical stress by 300~500 MPa under the same strain rate. But more significant effects come from the strain rates: from the calculations of a series of samples, we can see that $\log_{10}$(critical stress) and $\log_{10}$(strain rate) have approximate linear relations; if we extrapolate the strain rate to the

experimental value (10^{-2} s^{-1}), the critical nucleation stress could be in the range from $10^{2.8}$ to $10^{3.0}$ MPa (600 ~ 1000 MPa), which is almost the same as the experimental observations.

Here we must emphasis that these MD simulations cannot repeat the process of dense nanotwin array formation as our experiments. The main reason is also from the strain-rate effects. As shown in our kMC model, the formation of nanotwin array results from the correlated nucleation process, which is a kinetic phenomenon highly dependent on the strain rate. All our MD calculations can only be performed at extremely high strain rates compared with experiments, so it may reveal the deformation mechanism and dynamics of deformation twinning, but cannot produce the correct kinetics under low strain-rates.

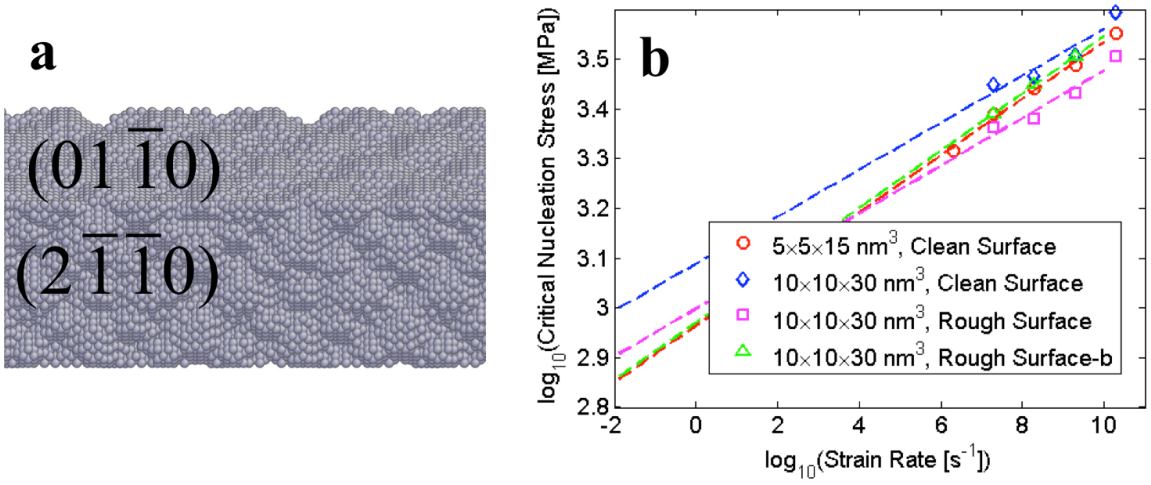

Figure S9 (a) MD sample with rough surfaces of $(2\bar{1}\bar{1}0)$ *and* $(01\bar{1}0)$ *and periodic boundary conditions along* $<0001>$ *directions. (b) Changes of critical nucleation stress of deformation twinning with strain rates for samples with different sizes, surface conditions and EAM potentials. Here except that the "10×10×30 nm^3, Rough Surface-b" sample was performed with potential from Ref. 7, all other samples were tested with potential from Ref. 4.*

9. Strain analysis of twin nucleation

The overall strain contribution of these nanotwins can be roughly estimated as follows: from the TEM images after the test we can roughly estimate the volume fraction of

twinned regions, where the average is ~50%. If we consider the $\{10\bar{1}2\}<10\bar{1}\bar{1}>$ twin in Mg, the shear strain along $<10\bar{1}\bar{1}>$ direction is theoretically 0.12. The overall strain along the C axis that would then be generated by these nanotwins is ~5%, a significant part of the total strain (total plastic strain ~20%). The twins contribute a large portion of the total strain because of the small sample volume and the large number of nanotwins (50% volume fraction in this example). Thus, these nanotwins play dual roles: they provide plastic strain and also facilitate subsequent dislocation plasticity because that the high density of twin boundaries can increase the dislocation storage and result in strain hardening. As an example of this, Figure 2b in main text is a BF TEM image of the nanotwin structure showing strong strain contrast in the twins, indicating a high density of dislocations in the twinned regions.

Reference:

(1) A. A. Luo, R. K. Mishra, A. K. Sachdev, *Metallurgical and Materials Transictions*. **41A**, 2662-2674(2010).

(2) M Kunz, et al. *Review of Scientific Instruments*. **80**, 035108-035118(2009).

(3) D. Kiener, A. M. Minor, *Acta Materialia***. 59**, 1328-1337(2010).

(4) X. Y. Liu, J. B. Adams, F. Ercolessi et al., *Modelling and Simulation in Materials Science and Engineering* **4** (3), 293 (1996).

(5) J. Wang, J. P. Hirth, and C. N. Tome, *Acta Materialia,* **57** (18), 5521 (2009).

(6) G. Kresse, J. Furthmuller, *Computational Materials Science,* **6**, 15 (1996).

(7) D. Y. Sun, M. I. Mendelev, C. A. Becker, et al., Physical Review *B,* **73**, 024116 (2006).